Nonlinear intelligent DC grid stabilization for fuel cell vehicle applications with a supercapacitor storage device

Phatiphat Thounthong [a,*], Luigi Piegari [b], Serge Pierfederici [c], Bernard Davat [c]

[a] Renewable Energy Research Centre, Department of Teacher Training in Electrical Engineering, Faculty of Technical Education, King Mongkut's University of Technology North Bangkok, 1518, Pracharat 1 Road, Bangsue, Bangkok 10800, Thailand

[b] Department of Electrical Engineering, Politecnico di Milano, Piazza Leonardo, 32, I-20133 Milan, Italy

[c] Groupe de Recherche en Electrotechnique et Electronique de Nancy, Université de Lorraine, 2, Avenue de la Forêt de Haye, Vandœuvre-lés-Nancy, Lorraine 54516, France

Received 1 August 2013
Received in revised form 25 July 2014
Accepted 28 July 2014

Introduction

Hydrogen fuel cells are a well-known and broadly applied power technology. Chosen for their high power density, FCs have provided electric power to both vehicles (space missions, city buses, submarines, tram, or locomotives), as depicted in Fig. 1, and power-plant applications (home and network) [1,2].

The PEMFC hydrogen utilization U is directly proportional to the current I and can be defined as:

$$U = \frac{I}{\dot{m} \cdot nF} \tag{1}$$

where $\dot{m}$ is the hydrogen flow rate, and nF is the charge flow between the anode and the cathode. Therefore, the hydrogen utilization closely follows the FC current and increases significantly at higher load currents.

For clarity, Fig. 2 presents a PEMFC stack (0.5 kW) used for testing. The oscilloscope waveforms in Fig. 3 depict the dynamic characteristics of the PEMFC (Fig. 2), illustrating the FC voltage and current. It shows the FC current transients due to variations in the power demands of the load. Because a PEMFC (like other FCs) is not a rigid voltage source, its voltage level decreases with an increase in the current demand. As depicted in Fig. 3, a voltage drop occurs in the voltage curve in Fig. 3(a) that is not observed in Fig. 3(b) because fuel flows have difficulties following a current step [3]. This behavior in the FC stack is called the "Fuel Starvation Phenomenon" [4,5]. This operating condition is evidently harmful to the FC stack, as demonstrated in [5], degrading the cell performance and ultimately shortening the life of the stack. Thus, to utilize an FC in dynamic applications, its current or power slope must be limited, as shown in Fig. 3(b).

* Corresponding author. Tel.: +66 2 913 2500x3332; fax: +66 2 587 8255.
E-mail address: phtt@kmutnb.ac.th (P. Thounthong).

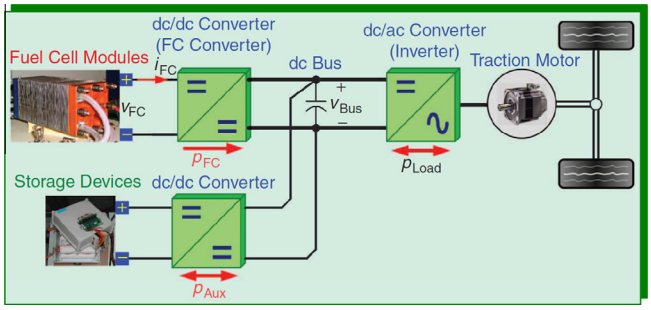

Fig. 1. Fuel cell-powered vehicle.

As a result, FCs must be combined with, at least, an intermediate energy storage element that possesses sufficient energy and the capability to deliver large amounts of power. Previous research has shown that FC hybridization with a battery or a supercapacitor (ultracapacitor) provides cost, performance, and operational improvements, as well as fuel economy benefits that are attractive and should be considered [6,7]. A battery is not the best choice for integration with an FC in a power quality system because of its sensitivity to temperature, maintenance issues, and its limited cycle life. For this application, supercapacitors are chosen as the energy storage device.

The cost effectiveness of the hybrid systems between FC/supercapacitor power source and FC/Li-Ion battery power source has been detailed by Thounthong and Raël [7]. It is beyond the scope of this paper to present the economic issue here. In this paper, the power converter structures and control methods are presented as follows. Power electronic converters play a significant role in electric systems. An FC is usually connected to the dc bus by a boost converter [8], and a storage device is connected to the dc bus by a two-quadrant dc/dc converter [9]. This type of system is a multi-converter structure and exhibits nonlinear behavior. Con-troller design methods can be placed into one of two categories: linear and nonlinear [10,11].

With most control techniques, a mathematical model of the system is used to obtain a solution to the feedback regulation problems. The most common structure is a linear structure in which the properties of a linear control system can be used. If the system in question is nonlinear, obtaining acceptable results is possible using various linearization techniques around different operating points [12,13]. However, there are situations in which this technique offers limited performance. Such situations may include a requirement for tight tracking of the reference signal in spite of large and sudden load variations or fast and smooth equilibrium-to-equilibrium transfers of the converters.

In recent years, the study of small-signal and large-signal stabilities of power switching converters based on its nonlinear nature

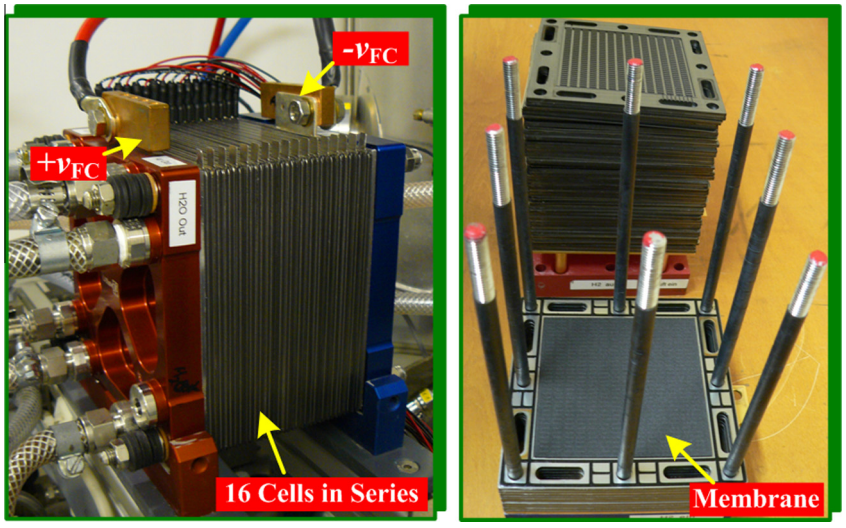

Fig. 2. PEM fuel cell (0.5 kW, 50 A, 16 cells in series) (in the GREEN Lab, Université de Lorraine, France) developed by the ZSW Company, Germany.

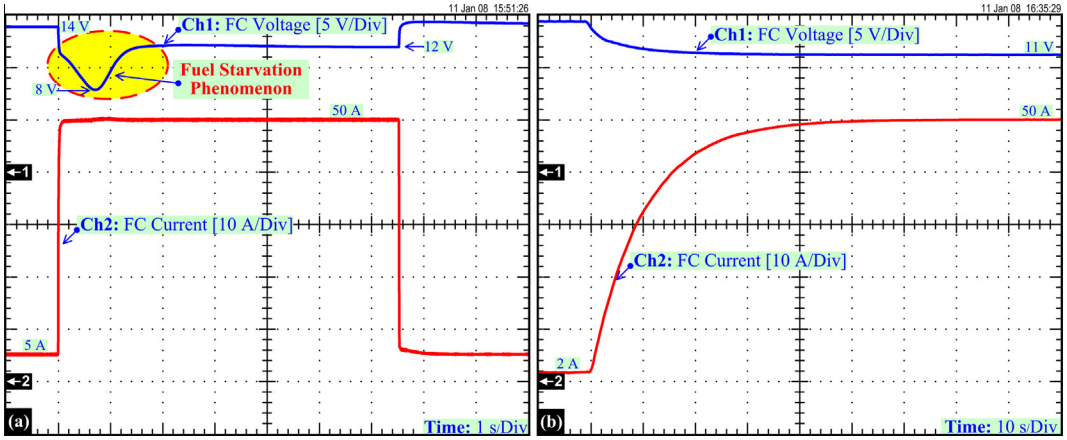

Fig. 3. PEMFC dynamic characteristics to: (a) current step and (b) controlled current slope.

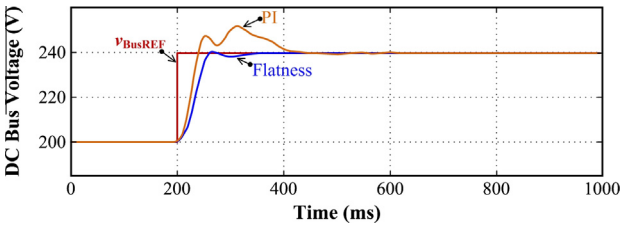

Fig. 4. Experimental results: comparison of the flatness-based control law with a linear PI control law for a dc bus voltage regulation during a step of dc bus voltage set-point v_{BusREF} at t = 200 ms from 200 V to 240 V [15].

has become one of the most important and complicated topics in the field of power electronics. The differential flatness theory was introduced by Fliess et al. [14] in 1995. More recently, these ideas have been used in a variety of power electronic systems and power systems [15,16]. One major property of differential flat systems is that all state and input variables can be expressed in terms of the flat output and a finite number of its derivatives without integrating any differential equation.

At least, Fig. 4 shows a comparison of the flatness-based and traditional linear proportional-integral (PI) control methods (vector control), which uses a dc bus voltage regulation in a three-phase voltage source converter (AC-to-DC converter) to step a dc bus voltage reference v_{BusREF}, as demonstrated by Song et al. [15]. The parameters of the linear controller were tuned to obtain the best possible performance. Fig. 4 shows the real experimental results obtained for both controllers during a set-point step. The flatness-based control shows good stability and an optimum response during dc bus voltage regulation. Using this data, one can conclude that the flatness-based control method provides bet-ter performance as compared to the classic PI controller.

Recently, several researchers [17–19] have proposed power electronic control design methods based on the fuzzy control theory which provides an alternative approach for collecting human knowledge and dealing with nonlinearities or uncertainties. The fuzzy control principle has succeeded in controlling complex nonlinear, incompletely modeled or uncertain systems that are not amenable to conventional control techniques [20,21]. Moreover, a Takagi–Sugeno (T–S) fuzzy model uses a set of fuzzy rules to approximate a nonlinear system in terms of a set of local linear models which are smoothly connected by fuzzy membership functions. The T–S fuzzy model has recently found extensive applications because its consequence part is an affine dynamic model rather than a fuzzy set.

In this paper, an intelligent-control (T–S fuzzy logic) law based on a differential flatness estimate of the system is proposed. This approach will provide a significant contribution to the field of hybrid power plants, particularly in nonlinear power electronics applications. The remainder of the paper is structured as follows: the next section describes the hybrid energy system and the power plant model that are studied in this work. In Section 'Control of a hybrid power source', a proof of the flat system consisting of the FC energy power plant, the fuzzy logic control law for DC link regulation and the supercapacitor charging strategy are presented. In Section 'Experimental validation', the test bench results for the proposed system are presented. Finally, this paper ends with concluding remarks for further study in Section 'Conclusion'.

Fuel cell/supercapacitor hybrid power plant

Proposed converter structure

There are many possible structures with which to connect a main source and a storage device to the utility dc bus [22,23]. For example, Fig. 5 presents the power converter circuits in the Toyota Camry Hybrid MY2007. It composes of a main source con-verter (connected with an AC generator), a motor inverter (as a load) and a classical 2-quadrant converter for Ni–MH battery. The total mass, volume, cost and efficiency (optimization) of the propulsion system are studied. One useful method is depicted in Fig. 6 [24,25], which consists of an FC converter and a supercapac-itor converter. This power converter connection is the good solu-tion when comparing the mass, volume and cost.

Multi-segment converters (Fig. 6) are proposed for high power applications [26]. The converters are connected to the output of the FC stack and the supercapacitor banks, which are subsequently connected in parallel to share the load. In high power applications, the number of parallel converter modules N would depend upon the rated power of the stack and the supercapacitor modules, where the subscript f is the number of parallel converters in the FC converter and c is the number of parallel converters in the supercapacitor converter. The use of parallel power converters (multiphase converters in parallel) with interleaving may offer better performance [27]. For the interleaving method, the converter modules all operate at the same switching frequency. Their switching waveforms are displaced in phase with respect to one another by $2\pi/N$ radians over the switching period, with N being the number of converters working in parallel.

For clarity, Fig. 7 shows the functional diagram of a two phase interleaved boost converter (N = 2). It is simply two boost converters in parallel operating 180° out of phase. The switching functions are generated by pulsewidth modulators PWM_1 and PWM_2, where T_S is the switching period. The modulation signals v_{C1} and v_{C2} are generated by a control circuit (the current control or power control loop). The carrier signals are triangular or saw tooth signals shifted by 180° (called the interleaving technique) and running at the same switching frequency f_S (= $1/T_S$). The input current i_{IN} (FC current or supercapacitor current) is the sum of the two inductor currents i_{L1} and i_{L2}. Because the inductor's ripple currents are out of phase, they tend to cancel each other and reduce the input ripple current caused by the boost inductors. The best input inductor ripple current cancellation occurs at 50 percent duty cycle. The

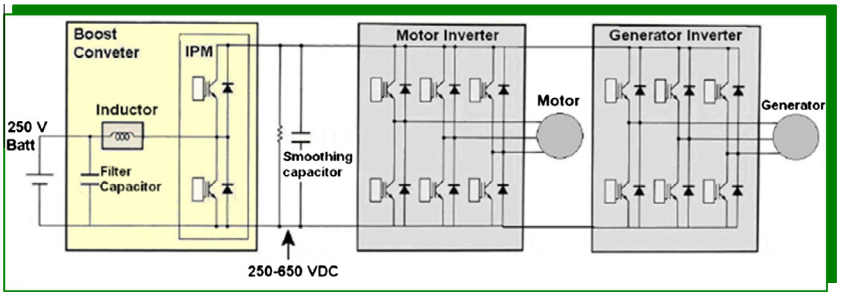

Fig. 5. Power converter circuits in the Toyota Camry Hybrid MY2007.

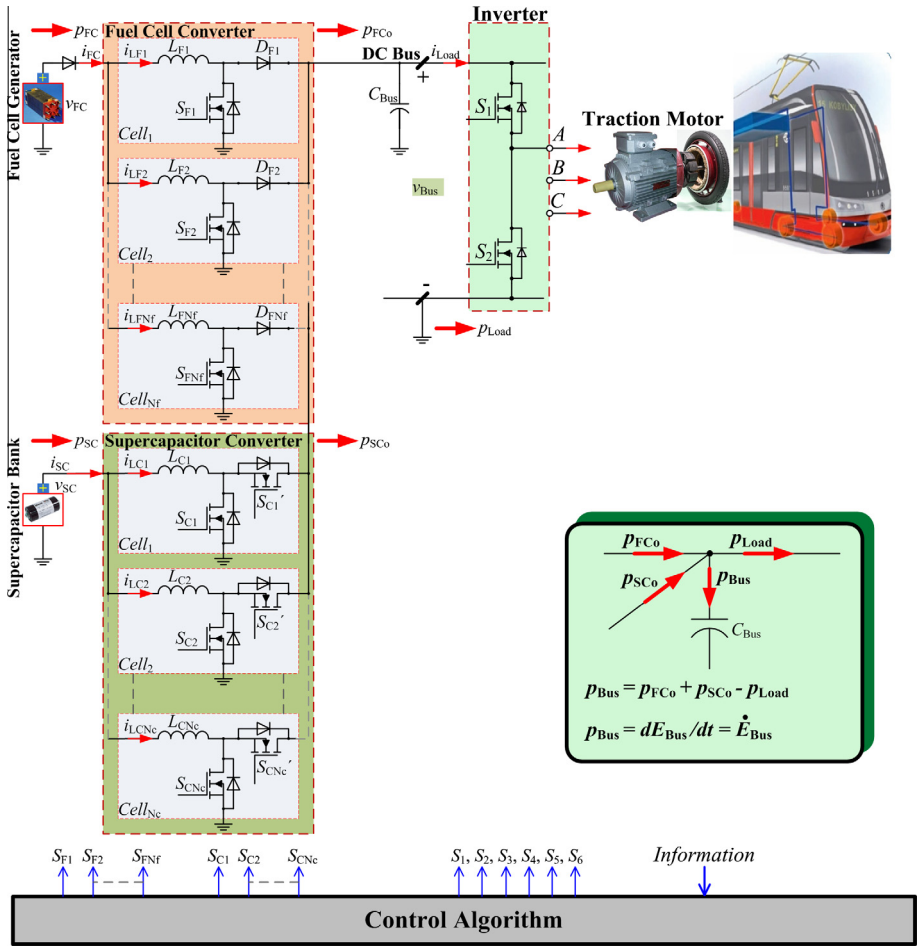

Fig. 6. Proposed multi-segment converters of a hybrid system supplied by a fuel cell and a supercapacitor, where p_{Load} (=$v_{Bus} \times i_{Load}$), v_{Bus}, and i_{Load} are the load power, the dc bus voltage, and the dc bus load current, respectively. p_{FC} (=$v_{FC} \times i_{FC}$), v_{FC}, and i_{FC} are the fuel cell power, voltage, and current, respectively. p_{SC} (=$v_{SC} \times i_{SC}$), v_{SC}, and i_{SC} are the supercapacitor power, voltage, and current, respectively. p_{FCo}, and p_{SCo} are the output powers to the DC link from the converters of the fuel cell and the supercapacitor, respectively.

benefits of this technique are associated with harmonic cancellation among the cells and include a low ripple amplitude and a high ripple frequency in the aggregate input and output waveforms [27].

For safety and high dynamics, these converters are primarily controlled by inner current regulation loops [26]. These current control loops are supplied by two reference signals: the supercapacitor reference current, i_{SCREF}, and the FC current reference i_{FCREF}, which are generated by the control algorithm presented in the next section.

Converter modeling

We assume that the FC and supercapacitor currents follow their reference values exactly. Thus,

$$i_{FC} = i_{FCREF} = \frac{p_{FC}}{v_{FC}} = \frac{p_{FCREF}}{v_{FC}} \tag{2}$$

$$i_{SC} = i_{SCREF} = \frac{p_{SC}}{v_{SC}} = \frac{p_{SCREF}}{v_{SC}}. \tag{3}$$

In these equations, the FC generator and the supercapacitor storage device function as controlled current sources. We assume that there are only static losses in these converters, and r_{FC} and r_{SC} represent the static losses in the FC and supercapacitor converters, respectively.

Because energy stored in the capacitor is much larger than that in the inductors, the electromagnetic energy stored in the inductors is neglected. The dc bus capacitive energy E_{Bus} and the supercapacitive energy E_{SC} can be written as:

$$E_{Bus} = \frac{1}{2} C_{Bus} v_{Bus}^2, \tag{4}$$

$$E_{SC} = \frac{1}{2} C_{SC} v_{SC}^2. \tag{5}$$

The total electrostatic energy E_T stored in the dc bus capacitor C_{Bus} and the supercapacitor C_{SC} can also be written as:

$$E_T = \frac{1}{2} C_{Bus} v_{Bus}^2 + \frac{1}{2} C_{SC} v_{SC}^2 \tag{6}$$

The dc bus capacitive energy E_{Bus} is given versus p_{FCo}, p_{SCo}, and p_{Load} by the following differential equation:

$$\dot{E}_{Bus} = p_{FCo} + p_{SCo} - p_{Load} \tag{7}$$

where

$$p_{FCo} = p_{FC} - r_{FC}\left(\frac{p_{FC}}{v_{FC}}\right)^2, \tag{8}$$

$$p_{SCo} = p_{SC} - r_{SC}\left(\frac{p_{SC}}{v_{SC}}\right)^2, \tag{9}$$

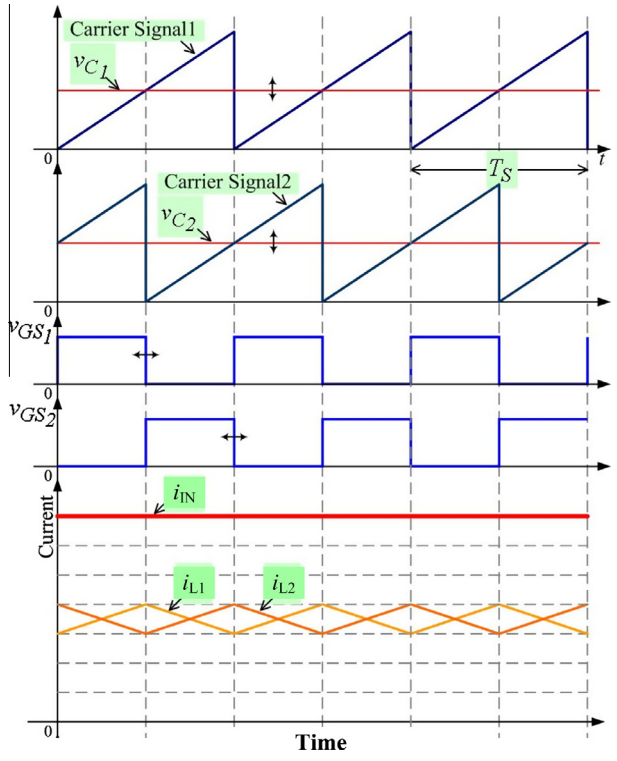

Fig. 7. Key waveforms of a two-phase interleaved boost converter ($N = 2$).

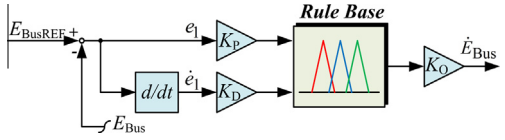

Fig. 8. Block diagram of fuzzy logic control, where K_P, K_D and K_O are the control parameters.

$$p_{Load} = \sqrt{\frac{2E_{Bus}}{C_{Bus}}} \cdot i_{Load}, \tag{10}$$

$$p_{SC} = \sqrt{\frac{2E_{SC}}{C_{SC}}} \cdot i_{SC}. \tag{11}$$

Control of a hybrid power source

Control algorithm

To manage the energy exchanges between the dc bus, the load, the FC main source, and the supercapacitor storage device, three operating modes (or states) can be identified [7].

(1) **Charge mode**, in which the main source supplies energy to the storage device and to the load.
(2) **Discharge mode**, in which both main source and storage device supply energy to the load.
(3) **Recovery mode**, in which the load supplies energy to the storage device.

The hybrid source control strategy presented hereafter is not based on the state definition, so naturally it presents no problem of chattering near state borders. We propose to function supercapacitors, which are the fastest energy source available for the proposed system, to supply the energy for the dc bus [26]. It is to say the dc bus energy regulation. The FC (as the slower dynamic device) functions to supply energy to both the dc bus capacitor C_{Bus} and the supercapacitors C_{SC} to maintain their charge. It is to say the supercapacitor energy regulation.

As a result, there are two voltage variables or two energy variables to be regulated [7]:

- The dc bus energy E_{Bus} is the most important variable.
- The supercapacitor storage energy E_{SC} is of secondary importance.

Thus, in this system, there are two energy controllers. The first one is the dc bus energy controller and the second one is the supercapacitor energy controller. These two controllers generate the power references: the supercapacitor power reference p_{SCREF} and the FC power reference p_{FCREF}, which are presented in the following paragraph.

In this study, the flat output [27] $\boldsymbol{y} = [y_1, y_2]^T$, the control variable $\boldsymbol{u} = [u_1, u_2]^T$, and the state variable $\boldsymbol{x} = [x_1, x_2]^T$ are defined as:

$$y = \begin{bmatrix} E_{Bus} \\ E_T \end{bmatrix}, \quad u = \begin{bmatrix} p_{SCREF} \\ p_{FCDem} \end{bmatrix}, \quad x = \begin{bmatrix} v_{Bus} \\ v_{SC} \end{bmatrix} \tag{12}$$

where p_{SCREF} is the supercapacitor power reference (set-point) and p_{FCDem} is the FC power demand.

From (4)–(6), the state variables $\boldsymbol{x}$ can be written as:

$$x_1 = \sqrt{\frac{2y_1}{C_{Bus}}} = \phi_1(y_1), \tag{13}$$

$$x_2 = \sqrt{\frac{2(y_2 - y_1)}{C_{SC}}} = \phi_2(y_1, y_2). \tag{14}$$

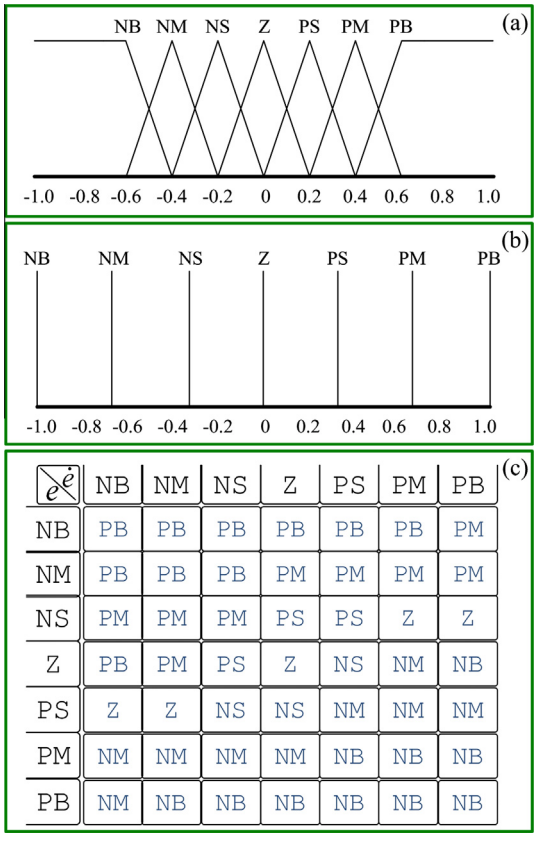

e \ $\dot{e}$	NB	NM	NS	Z	PS	PM	PB
NB	PB	PB	PB	PB	PB	PB	PM
NM	PB	PB	PB	PM	PM	PM	PM
NS	PM	PM	PM	PS	PS	Z	Z
Z	PB	PM	PS	Z	NS	NM	NB
PS	Z	Z	NS	NS	NM	NM	NM
PM	NM	NM	NM	NM	NB	NB	NB
PB	NM	NB	NB	NB	NB	NB	NB

Fig. 9. Rule base and membership functions, (a) input membership function, (b) output membership function and (c) rule base.

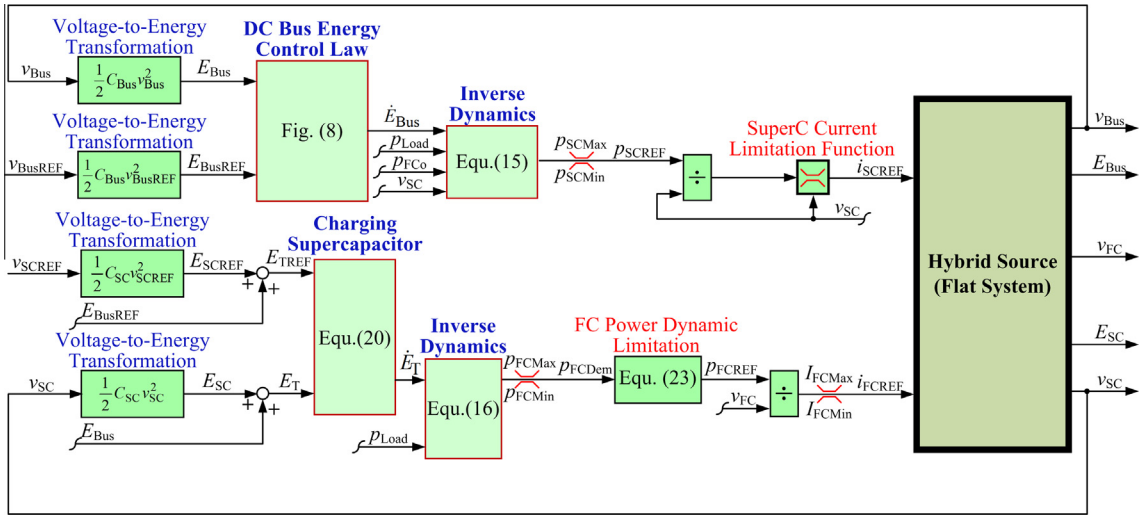

Fig. 10. Control structure of the FC/supercapacitor hybrid source.

Fig. 11. Test-bench system for the FC/supercapacitor power plant.

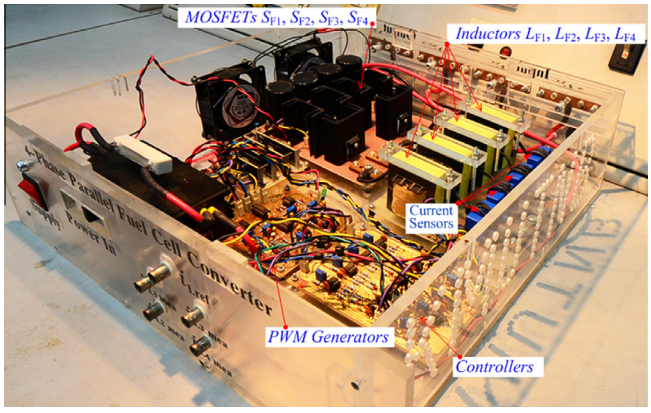

Fig. 12. Four-phase parallel interleaved FC converter (1200 W).

From (6)–(11), the input control variables $\boldsymbol{u}$ can be calculated from the flat output $\boldsymbol{y}$ and its time derivatives (*inverse dynamics*):

$$u_1 = 2p_{\mathrm{SCMax}} \cdot \left[1 - \sqrt{1 - \left(\frac{\dot{y}_1 + \sqrt{\frac{2y_1}{C_{\mathrm{Bus}}}} i_{\mathrm{Load}} - p_{\mathrm{FCo}}}{p_{\mathrm{SCMax}}}\right)}\right] = \psi_1(y_1, \dot{y}_1) = p_{\mathrm{SCREF}} \tag{15.1}$$

$$u_1 = \dot{y}_1 + \sqrt{\frac{2y_1}{C_{\mathrm{Bus}}}} \cdot i_{\mathrm{Load}} - p_{\mathrm{FC}} \Big|_{r_{\mathrm{FC}}=0,\ r_{\mathrm{SC}}=0} = \psi_1(y_1, \dot{y}_1) = p_{\mathrm{SCREF}} \tag{15.2}$$

$$u_2 = 2p_{\mathrm{FCMax}} \cdot \left[1 - \sqrt{1 - \left(\frac{\dot{y}_2 + \sqrt{\frac{2y_1}{C_{\mathrm{Bus}}}} i_{\mathrm{Load}}}{p_{\mathrm{FCMax}}}\right)}\right] = \psi_2(y_1, \dot{y}_2) = p_{\mathrm{FCDem}} \tag{16.1}$$

$$u_2 = \dot{y}_2 + \sqrt{\frac{2y_1}{C_{Bus}}} \cdot i_{Load} \Big|_{r_{FC}=0} = \psi_1(y_1, \dot{y}_2) = p_{FCDem} \quad (16.2)$$

where

$$p_{SCMax} = \frac{v_{SC}^2}{4r_{SC}}, \quad (17)$$

$$p_{FCMax} = \frac{v_{FC}^2}{4r_{FC}}. \quad (18)$$

In this case, p_{SCMax} and p_{FCMax} are the limited maximum power of the supercapacitor and FC sources, respectively.

Thus, it is clear that $x_1 = \phi_1(y_1)$, $x_2 = \phi_2(y_1, y_2)$, $u_1 = \psi_1(y_1, \dot{y}_1)$, and $u_2 = \psi_2(y_1, \dot{y}_2)$. Consequently, the proposed reduced order sys-tem can be studied as a flat system [28,29].

DC bus energy regulation based on fuzzy logic

A fuzzy logic controller (FLC) can be decomposed into three data processing parts: fuzzification, rule evaluation (inference engine), and defuzzification. The controller is based on fuzzy reasoning mapping between real-world information and numerical information [20,21]. As shown in many applications [30,31], the Mamdani inference method is the most commonly used inference technique. However, this method requires high performance in the computation process because the centroids of the membership functions must be obtained. In contrast, the Takagi–Sugeno (T–S) method with a singleton output provides a faster evaluation time, which has been used effectively in various studies [30,31]. It is also appropriate for real-time applications that need high-speed computing hardware, such as a DSP card or dSPACE. The control objective is to regulate the dc bus voltage v_{Bus} or the dc bus energy E_{Bus} (= y_1). The controller contains a Takagi–Sugeno inference engine and two fuzzy inputs: the energy error $e_1 (= y_{1REF} - y_1)$ and the dif-ferential energy error $\dot{e}_1$, which are carefully adjusted using the proportional gain K_P and the derivative gain K_D, respectively. In addition, the fuzzy output level can be set by the proportional gain K_O, as shown in Fig. 8.

Triangular and trapezoidal membership functions are chosen for both of the fuzzy inputs, as shown in Fig. 9(a). There are seven membership functions for each input, including *NB* (Negative Big), *NM* (Negative Medium), *NS* (Negative Small), *Z* (Zero), *PB* (Positive Big), *PM* (Positive Medium) and *PS* (Positive Small). For the singleton output membership function, the zero-order Sugeno model is used, where the membership functions are specified symmetrically, as follows: *NB* = −1, *NM* = −0.66, *NS* = −0.33, *Z* = 0, *PB* = 1, *PM* = 0.66, and *PS* = 0.33, as presented in Fig. 9(b).

For the rule base, expert suggestions, an experimental approach and a trial and error technique were used to define the relationships between the inputs and the output. The data representation was in the form of an IF-THEN rule, as shown in the following example:

IF(e_{1i}) is NS and $\dot{e}_{1i}$ is NS
THEN (z_i : output) is NB.(19)

As shown in Fig. 9(c), the total number of rule bases is therefore equal to 49 rules. To obtain the output of the controller, the center of gravity method for the *COGS* of the singletons is utilized as:

$$U = \frac{\sum_{i=1}^{N} w_i z_i}{\sum_{i=1}^{N} w_i} \quad (20)$$

where the weights (w_i) can be retrieved from

$$w_i = \max(e_{1i}, \dot{e}_{1i}). \quad (21)$$

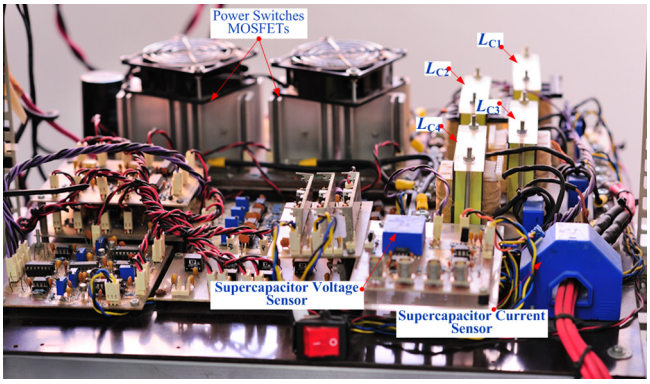

Fig. 13. Four-phase parallel interleaved supercapacitor converter (3000 W).

Table 1
Converter parameters and semiconductor devices.

Fuel cell converter:	
Inductors $L_{F1} = L_{F2} = L_{F3} = L_{F41}$	396 μH
MOSFETS $S_{F1} = S_{F2} = S_{F3} = S_{F4}$	IRFP264N: 250 V, 38 A
Diodes $D_{F1} = D_{F2} = D_{F3} = D_{F4}$	RURG3020: 200 V, 30 A
Supercapacitor converter:	
Inductors $L_{C1} = L_{C2} = L_{C3} = L_{C4}$	150 μH
MOSFETS $S_{C1} = S_{C2} = S_{C3} = S_{C4} = S'_{C1} = S'_{C2} = S'_{C3} = S'_{C4}$	IRFP264N: 250 V, 38 A

Table 2
DC-bus energy control loop parameters.

v_{BusREF}	60 V
C_{Bus}	12,200 μH
K_P	0.15
K_D	0.15
K_O	−200
r_{SC}	0.01 Ω
P_{SCMax}	+3750 W
P_{SCMin}	−3750 W
V_{SCMax}	32 V
V_{SCMin}	15 V
$I_{SCRated}$	150 A

Charging supercapacitor

For supercapacitor energy regulation, the desired reference for the total energy is represented by y_{2REF} (= y_{TREF}). Because the supercapacitor has an enormous energy storage capacity and the supercapacitor energy variable is defined as a slower dynamic variable than the dc bus energy variable, the total energy control law is defined as:

$$(\dot{y}_2 - \dot{y}_{2REF}) + K_{21}(y_2 - y_{2REF}) = 0 \quad (22)$$

If we define $e_2 = y_2 - y_{2REF}$ and $K_{21} = 1/\tau_S$, we obtain:

Table 3
Charging supercapacitor control loop parameters.

v_{SCREF}	25 V
C_{SC}	100 F
K_{21}	0.1
r_{FC}	0.1 Ω
P_{FCMax}	600 W
P_{FCMin}	0 W
I_{FCMax} (Rated)	46 A
I_{FCMin}	0 A
ω_n	0.4 rad s^{-1}
ζ	1 p.u.

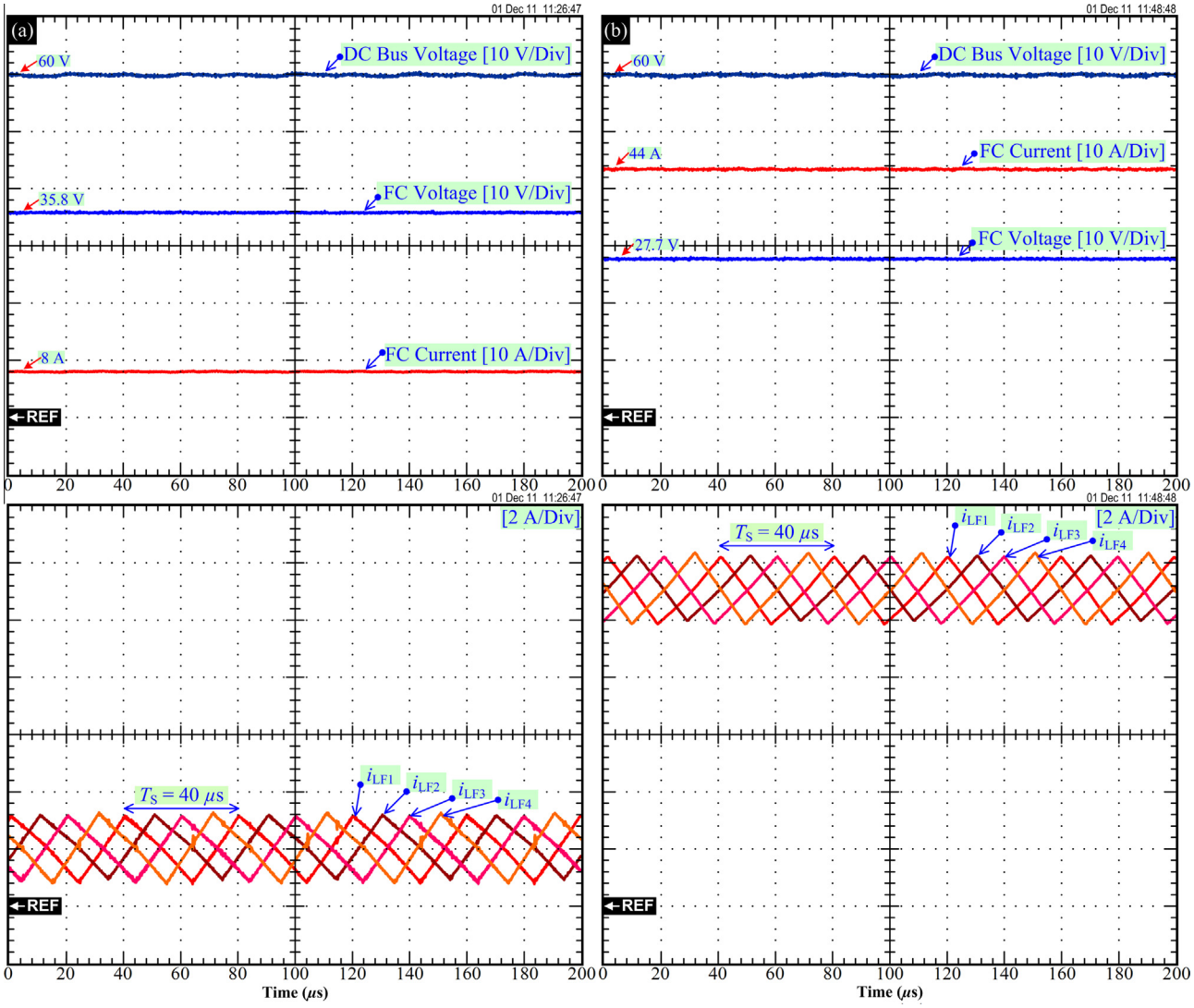

Fig. 14. Experimental results: steady-state waveforms of the FC interleaved converter system at an FC current command of (a) 8 A and (b) 44 A.

$$\tau_S \cdot \dot{e}_2 + e_2 = 0. \tag{23}$$

Substituting the expression for $\dot{y}_2$ from (20) into (16.1) gives the equation for the closed-loop static state feedback FC power, as follows:

$$u_2 = 2p_{FCMax} \cdot \left[1 - \sqrt{1 - \left(\frac{[\dot{y}_{2REF} + K_{21}(y_{2REF} - y_2)] + \sqrt{\frac{2y_1}{C_{Bus}}} i_{Load}}{p_{FCMax}}\right)}\right] = p_{FCDem} \tag{24}$$

Conclusion of the control algorithm

The multivariable control of the FC/supercapacitor hybrid power source detailed above is portrayed in Fig. 10. The dc bus energy-control law (the intelligent fuzzy logic) generates a supercapacitor power reference p_{SCREF}. This signal is subsequently divided by the measured supercapacitor voltage v_{SC} and limited to maintain the supercapacitor voltage within an interval [V_{SCMin}, V_{SCMax}] by limiting the supercapacitor charging current or discharging current, as presented in the block "SuperC Current Limitation Function" [32]. This results in the supercapacitor current reference i_{SCREF}.

The supercapacitor energy control law generates the FC power demand p_{FCDem}. It must be limited to maintain the FC power within an interval [p_{FCMin}, p_{FCMax}] and must also be limited in slope, which enables the safe operation of the FC with respect to the dynamic constraints that are associated with the FC stack. Therefore, to limit the transient FC power, a low-pass filter (second order) is employed such that the power demand p_{FCDem} from the external loop is always limited (desired trajectory planning) by:

$$p_{FCREF}(t) = p_{FCDem}(t) \cdot (1 - e^{-\frac{t}{\tau_1}} - \frac{t}{\tau_1} e^{-\frac{t}{\tau_1}}) \tag{25}$$

where τ_1 is the control parameter.

Experimental validation

Platform description

To validate the proposed control algorithm and control laws, a small-scale test bench of the hybrid system was implemented in our laboratory, as presented in Figs. 11–13. The FC system used in this effort was a PEMFC system (1.2 kW, 46 A; Ballard Power Systems Company). The supercapacitor module (100 F, 32 V; Maxwell Technologies Company) consisted of 12 BCAP1200 cells

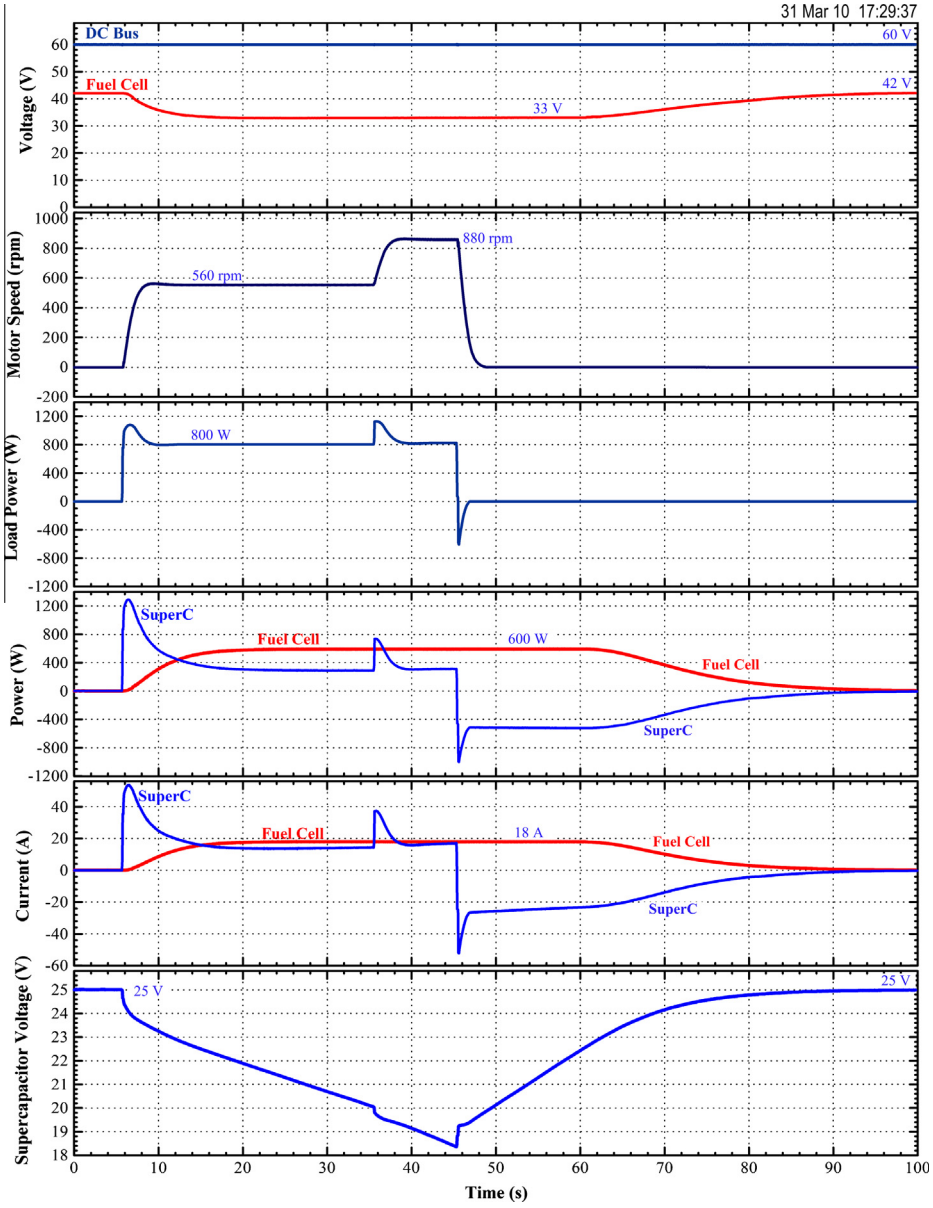

Fig. 15. Experimental results for hybrid source during motor drive cycle.

(1200 F; 2.7 V) connected in series. The FC converter (1.2 kW, 4-phase interleaved) and the supercapacitor converter (3 kW, 4-phase interleaved) (refer to Fig. 6) were both constructed in the laboratory, as presented in Figs. 12 and 13 and Table 1.

Control description

The FC current i_{FC}, the supercapacitor current i_{SC}, the load current i_{Load}, the dc bus voltage v_{Bus}, the FC voltage v_{FC}, and the supercapacitor voltage v_{SC} were measured by zero-flux Hall effect sensors. The FC and supercapacitor current regulation loops were constructed using analogue circuits functioning at a high bandwidth. The parameters associated with the dc-bus energy regulation loop and the charging supercapacitor regulation loop are presented in Tables 2 and 3, respectively. The FC power dynamic delay is shown in Table 3. This value was experimentally shown to have the highest power slope for this FC system at which no fuel starvation occurs. It must be noted that for the small-scale test bench, the maximum FC power p_{FCMax} was set at 600 W, and the rated FC power considered in this experiment was 1200 W. These two energy control loops, which generated the current references i_{FCREF} and i_{SCREF}, were implemented in the real-time dSPACE DS1104 card using MATLAB–Simulink at a sampling frequency of 25 kHz.

Experimental results

The dc bus voltage of 60 V was connected to an electronic load and a traction motor that was coupled with a small inertia flywheel and a powder brake, which is independent of the mechanical speed. The oscilloscope waveforms in Fig. 14 portray the steady-state characteristics of the four-phase interleaved FC converters at different FC current demands. It demonstrates the dc bus volt-age, the FC voltage, the FC current, the first, second, third and forth inductor currents. Fig. 14(a) and (b) presents the characteristics at the average FC current reference of 8 A and 44 A, respectively. One can observe that the FC current is the sum of the inductor currents and that the FC ripple current is 1/N the individual inductor ripple

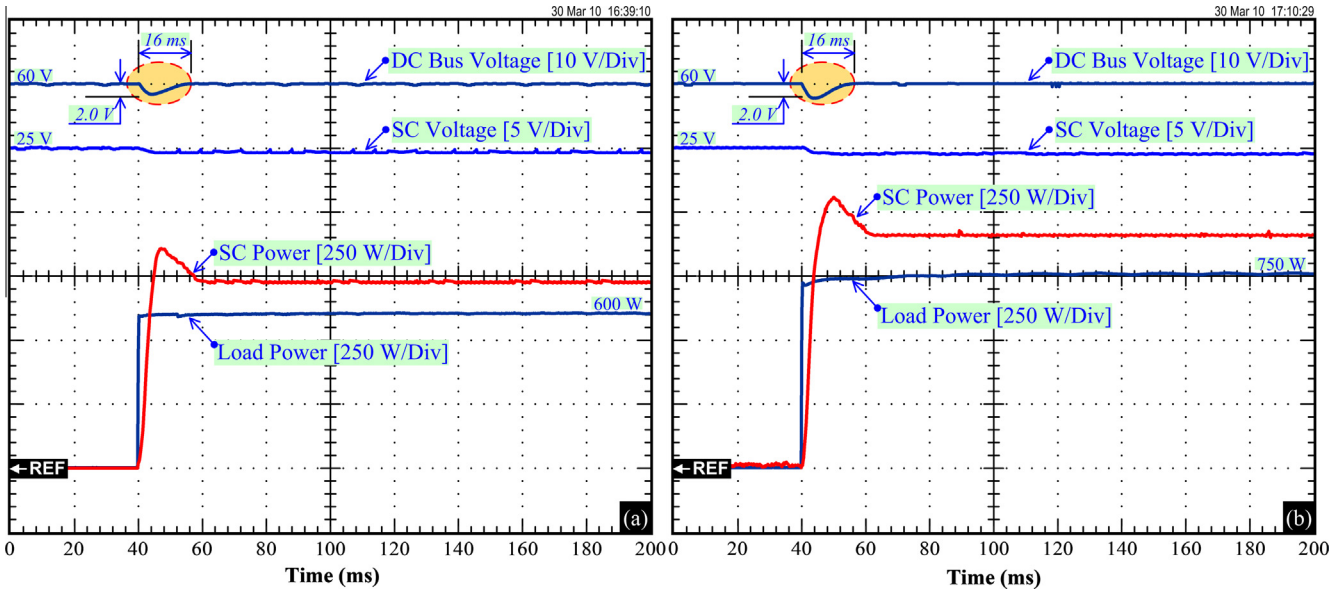

Fig. 16. Experimental results of the dynamic characteristics of the hybrid source during a step load from: (a) 0–600 W and (b) 0–750 W.

currents. So, the FC ripple current of the four-cell interleaved converter is nearly zero. It means that the FC mean current is close to the FC rms current.

The waveforms that were obtained during the motor drive cycle are presented in Fig. 15. The data show the dc bus voltage, the fuel cell voltage, the motor speed, the load power (=the motor power), the supercapacitor power, the fuel cell power, the supercapacitor current, the fuel cell current, and the supercapacitor voltage (or the supercapacitor *SOC*). At the initial state, the load power is zero (the motor is stopped), and the storage device is fully charged, i.e., $v_{SC} = 25$ V; as a result, both the fuel cell and supercapacitor powers are zero. At $t = 6$ s, the traction motor speed accelerated to its final speed of 560 r/min. The following observations are made:

- The supercapacitor, which supplies most of the power that is required during motor acceleration, remained in a discharged state after the start of the motor because the steady state load power (friction load) is greater than the FC-limited maximum power.
- Simultaneously, the final FC power increased with a limited slope [refer to (23)] to its limited maximum power of 600 W.

Next, at $t = 35$ s, the motor speed accelerated from 560 r/min to its final speed of 880 r/min. Because the FC power was at its limited maximum power of 600 W, the supercapacitor supplies most of the power that is required during motor acceleration and was deeply discharged.

At $t = 45$ s, the supercapacitor voltage is equal to 18.5 V, which means that the supercapacitor supplies its stored energy E_{SC} to the dc bus. This energy E_{SC_Supply} is estimated to be:

$$E_{SC\_Supply} = \tfrac{1}{2} \cdot C_{SC} \cdot v_{SC}^2(t = 6\text{ s}) - \tfrac{1}{2} \cdot C_{SC} \cdot v_{SC}^2(t = 45\text{ s}) = 3.925\text{ Wh}$$

The motor speed then decelerated to a stop with a peak load power of approximately −600 W. As a result, the supercapacitor changes from discharging to charging and demonstrates the following four phases:

- First, the supercapacitor is charged by the fuel cell (600 W) and the motor (the regenerative braking energy).
- Second, the load power is zero, and the supercapacitor is only charged by the fuel cell at 600 W.
- Third, at $t = 62$ s, the supercapacitor is nearly fully charged, i.e., $v_{SC} = 23.0$ V. As a result, the fuel cell power is reduced with limited power dynamics.
- Finally, at $t = 89$ s, the supercapacitor is fully charged, i.e., $v_{SC} = v_{SCREF} = 25$ V. After slowly decreasing, the fuel cell and supercapacitor powers are zero.

It is evident that the dc bus voltage waveform is asymptotically stable during the large load cycles (the motor drive cycles), which is of major importance when using a supercapacitor to improve the dynamic performance of the whole system using the proposed fuzzy-logic controller for DC link regulation.

To demonstrate dc bus voltage control by the intelligent fuzzy-logic controller (refer to Fig. 8), the oscilloscope waveforms in Fig. 16 show the response of the dc bus voltage dynamics (representing the flat output y_1) to the large load power demands (disturbance) from 0 to 600 W and from 0 to 750 W when the dc bus was loaded with an electronic load. The oscilloscope screens show the dc bus voltage (the state variable x_1, representing the flat output y_1), the supercapacitor voltage (the state variable x_2), the load power, and the supercapacitor power (the control input variable u_1).

The fuel cell power dynamics were purposely limited (see Fig. 3), forcing the supercapacitor to supply the transient load power demand. The proposed fuzzy-logic controller shows good stability and an optimum response (*no oscillation* and *short settling time*) for the regulation of the dc bus voltage to the desired reference of 60 V.

Note that there are some losses (static and dynamic) in the supercapacitor converter (see Fig. 6) because the converters are hard-switching converters; therefore, a power difference can be observed between the supercapacitor power and the load power, for example, in the 40 to 200 ms range. To improve the converter efficiency, soft-switching converters may be an effective solution for future projects.

Conclusion

This paper proposes an intelligent control law for DC link regulation for a power plant supplied by an FC main source and a supercapacitor supplementary source for hydrogen vehicle applications. In particular, we do not restrict ourselves to linear

control techniques at an equilibrium point. The main contribution of this paper is the implementation and experimental validation of T–S fuzzy control based on the differential flatness approach for dc bus voltage control (energy balance). We study a simple control system for the power plant based upon the physical structure of the model. This study represents novel work in this domain.

Experimental verification with a small-scale power plant (Nexa Ballard FC power generator: 1.2 kW, 46A; Maxwell supercapacitor storage device: 100 F, 32 V) demonstrated excellent performance by the whole system and validates the proposed energy-management principle. Nevertheless, the proposed control law requires a current-load measurement to calculate the load power. For future work, a load observer will be used to avoid a direct measurement of the load current, as was explored in [16], which is called a sensorless load observer.

Acknowledgments

This research work was financially supported by the Office of the Higher Education Commission of Thailand and King Mongkut's University of Technology North Bangkok (KMUTNB), Thailand. Contract No. KMUTNB-NRU-57-08. The authors gratefully acknowledge the contributions of A. Luksanasakul and P. Koseeyaporn for their information on the fuzzy logic.

References

[1] Chang WY. Estimating equivalent circuit parameters of proton exchange membrane fuel cell using the current change method. Int J Electr Power Energy Syst 2013;53:584–91.
[2] Pinto PJR, Sousa T, Fernandes VR, Pinto AMFR, Rangel CM. Simulation of a stand-alone residential PEMFC power system with sodium borohydride as hydrogen source. Int J Electr Power Energy Syst 2013;49:57–65.
[3] Thounthong P, Davat B, Raël S, Sethakul P. Fuel starvation: analysis of a PEM fuel cell system. IEEE Ind Appl Mag 2009;15:52–9.
[4] Xiea C, Ogdenb JM, Quana S, Chena Q. Optimal power management for fuel cell–battery full hybrid powertrain on a test station. Int J Electr Power Energy Syst 2013;53:307–20.
[5] Taniguchi A, Akita T, Yasuda K, Miyazaki Y. Analysis of electrocatalyst degradation in PEMFC caused by cell reversal during fuel starvation. J Power Sources 2004;130:42–9.
[6] Bauman J, Kazerani M. A comparative study of fuel-cell–battery, fuel-cell–ultracapacitor, and fuel-cell–battery–ultracapacitor. IEEE Trans Veh Technol 2008;57(2):760–9.
[7] Thounthong P, Raël S. The benefits of hybridization: an investigation of fuel cell/battery and fuel cell/supercapacitor hybrid sources for vehicle applications. IEEE Ind Electron Mag 2009;3(3):25–37.
[8] Segura F, Andújar JM. Power management based on sliding control applied to fuel cell systems: a further step towards the hybrid control concept. Appl Energy 2012;99:213–25.
[9] Erdinc O, Uzunoglu M. Recent trends in PEM fuel cell-powered hybrid systems: investigation of application areas, design architectures and energy management approaches. Renew Sust Energy Rev 2010;14:2874–84.
[10] Bizon N. A new topology of fuel cell hybrid power source for efficient operation and high reliability. J Power Sources 2011;196:3260–70.
[11] Kumar L, Jain S. A multiple source DC/DC converter topology. Int J Electr Power Energy Syst 2013;51:278–91.
[12] Haruni AMO, Negnevitsky M, Haque ME, Gargoom A. A novel operation and control strategy for a standalone hybrid renewable power system. IEEE Trans Sust Energy 2013;4:402–13.
[13] Luo An, Chen Yandong, Shuai Zhikang, Chunming Tu. An Improved reactive current detection and power control method for single-phase photovoltaic grid-connected DG system. IEEE Trans Energy Convers 2013;28:823–31.
[14] Fliess M, Lévine J, Martin Ph, Rouchon P. A lie–bäcklund approach to equivalence and flatness of nonlinear systems. IEEE Trans Autom Contr 1999;44(5):922–37.
[15] Song E, Lynch AF, Dinavahi V. Experimental validation of nonlinear control for a voltage source converter. IEEE Trans Control Syst Technol 2009;17:1135–44.
[16] Variani MH, Tomsovic K. Distributed automatic generation control using flatness-based approach for high penetration of wind generation. IEEE Trans Power Syst 2013;28:3002–9.
[17] Jafarzadeh S, Fadali MS, Evrenosoglu CY. Solar power prediction using interval type-2 TSK modeling. IEEE Trans Sust Energy 2013;4:333–9.
[18] Celimuge Wu, Ohzahata S, Kato T. Flexible, portable, and practicable solution for routing in VANETs: a fuzzy constraint Q-learning approach. IEEE Trans Veh Technol 2013;62:4251–63.
[19] Masih-Tehrani M, Hairi-Yazdi MR, Esfahanian V, Safaei A. Optimum sizing and optimum energy management of a hybrid energy storage system for lithium battery life improvement. J Power Sources 2013;244:2–10.
[20] Takagi T, Sugeno M. Fuzzy identification of systems and its applications to modeling and control. IEEE Trans Syst, Man Cybern 1985;15(1):116–32.
[21] Johansen TA, Shorten R, Murray-Smith R. On the interpretation and identification of dynamic Takagi–Sugeno fuzzy models. IEEE Trans Fuzzy Syst 2000;8(3):297–313.
[22] Tan Xingguo, Li Qingmin, Wang Hui. Advances and trends of energy storage technology in Microgrid. Int J Electr Power Energy Syst 2013;44:179–91. Pan
[23] Chaofeng, Chen Long, Chen Liao, Huang Chen, Xie Meizhi. Research on energy management of dual energy storage system based on the simulation of urban driving schedules. Int J Electr Power Energy Syst 2013;44:37–42.
[24] Feroldi D, Serra M, Riera J. Design and analysis of fuel-cell hybrid systems oriented to automotive applications. IEEE Trans Veh Technol 2009;58(9):4720–9.
[25] Bernard J, Delprat S, Büchi FN, Guerra TM. Fuel-cell hybrid powertrain: toward minimization of hydrogen consumption. IEEE Trans Veh Technol 2009;58(7):3168–76.
[26] Thounthong P, Pierfederici S, Martin J-Ph, Hinaje M, Davat B. Modeling and control of fuel cell/supercapacitor hybrid source based on differential flatness control. IEEE Trans Veh Technol 2010;59(6):2700–10.
[27] Thounthong P, Pierfederici S. A new control law based on the differential flatness principle for multiphase interleaved DC–DC converter. IEEE Trans Circ Syst II Express Briefs 2010;57:903–7.
[28] Danzer MA, Wilhelm J, Aschemann H, Hofer EP. Model-based control of cathode pressure and oxygen excess ratio of a PEM fuel cell system. J Power Sources 2008;176:515–22.
[29] Payman A, Pierfederici S, Meibody-Tabar F. Energy control of supercapacitor/fuel cell hybrid power source. Energy Convers Manag 2008;49:1637–44.
[30] Thounthong P, Luksanasakul A, Koseeyaporn P, Davat B. Intelligent model-based control of a standalone photovoltaic/fuel cell power plant with supercapacitor energy storage. IEEE Trans Sust Energy 2013;4:240–9.
[31] Benbouzid MElH, Diallo D, Zeraoulia M. Advanced fault-tolerant control of induction-motor drives for EV/HEV traction applications: from conventional to modern and intelligent control techniques. IEEE Trans Veh Technol 2007;56(2):519–28.
[32] Thounthong P, Raël S, Davat B. Control algorithm of fuel cell and batteries for distributed generation system. IEEE Trans Energy Convers 2008;23:148–55.